Chemical Science

ROYAL SOCIETY OF CHEMISTRY

EDGE ARTICLE

View Article Online
View Journal | View Issue

Cite this: *Chem. Sci.*, 2021, **12**, 8548

All publication charges for this article have been paid for by the Royal Society of Chemistry

A new strategy for constructing a dispiro-based dopant-free hole-transporting material: spatial configuration of spiro-bifluorene changes from a perpendicular to parallel arrangement†

Zhongquan Wan, *[a] Jinyu Yang,[a] Jianxing Xia,[a] Hongyu Shu,[a] Xiaojun Yao, [b] Junsheng Luo[a] and Chunyang Jia *[a]

Received 10th March 2021
Accepted 12th May 2021

DOI: 10.1039/d1sc01416a

rsc.li/chemical-science

Due to the low intrinsic hole mobility caused by the orthogonal conformation of two fluorene units in Spiro-OMeTAD which is a classic hole-transporting material (HTM) in perovskite solar cells (PSCs), Spiro-OMeTAD based PSCs generally can only obtain high performances through a sophisticated doping process with dopants/additives, which adds to the cost and complicacy of device fabrication, and also adversely affects the stability of PSC devices. Herein, a novel dispiro-based HTM, WH-1, is designed by cleverly replacing the central carbon atom of Spiro-OMeTAD with cyclohexane, and the spatial configuration of the HTM is changed from vertical orthogonality of the two fluorene units to a parallel arrangement, which is beneficial for the formation of a homogeneous and compact HTM film on the surface of the perovskite film, improvement of intermolecular electronic coupling and intrinsic hole mobility. WH-1 is obtained by two-step facile synthesis with a high yield from commercially available materials. WH-1 is used in PSCs as a dopant-free HTM, which is the first time that the dispiro-based molecule has been applied as a dopant-free HTM, and a power conversion efficiency (PCE) of 19.57% is obtained, rivaling Li-TFSI/*t*-BP doped Spiro-OMeTAD in PCE (20.29%), and showing obvious superior long-term stability.

Introduction

As a kind of photovoltaic cell with great development prospects, hybrid organic-inorganic halide perovskite solar cells (PSCs) have attracted intense attention. From 2009 until now, the power conversion efficiencies (PCEs) of PSCs have been improving fiercely from 3.8% to 25.5%.[1–4] In the multilayer structure of PSCs, the hole-transporting material (HTM) layer located between the perovskite film and metal electrode plays a crucial role in extracting holes and blocking electrons.[5] In many types of HTMs, organic small molecules have been widely designed and used in PSCs because of the advantages of the facile solution process, controllable molecular structure, and easy preparation and purification.[6–10] The monospiro-based organic small molecule material 2,2′,7,7′-tetrakis-(*N*,*N*-di-*p*-methoxyphenylamine)-9,9′-spiro-bifluorene (Spiro-OMeTAD) is still the most classic HTM in PSCs so far, which features two fluorene units linked by an orthogonal molecular conformation, owing to its advantages in solubility, film-forming and thermal stability.[11]

Due to the successful application of Spiro-OMeTAD in PSCs, the HTMs based on a spiro-structure have been widely concerned. In the past few years, various HTMs with a spiro-structure were designed and synthesized by regulating the spiro-core, and the photovoltaic performances were improved.[12–20] Two spiro-HTMs called X-59 and X-60 (Fig. S1†) were constructed based on a spiro[fluorene-9,9′-xanthene] (SFX) as a skeleton by Sun *et al.*, and PCEs of 19.80% and 19.84% were obtained, respectively.[13,14] Nazeeruddin *et al.* used a spiro[cyclopenta[2,1-*b*:3,4-*b*′]dithiophene-4,9′-fluorene] unit to build a new HTM FDT for PSCs, which achieved an attractive PCE of 20.2%.[15] Lately, many dispiro-based molecules with more complex structures have also been studied to explore their feasibility as HTMs in PSCs. Sun *et al.* used two SFX cores to exploit two HTMs X-26 and X-36 with a dispiro-based structure, and satisfactory PCEs of 20.2% and 18.9% were obtained, respectively.[16] Two other dispiro-based HTMs G1 and G2 were reported by Jen *et al.*, and showed very significant PCEs of 15.5% and 20.2%, respectively.[17] Although some dispiro-based HTMs also exhibit outstanding photovoltaic performances in PSCs, their molecular structures are evidently more complicated compared with those of monospiro systems, and their synthesis

[a]*State Key Laboratory of Electronic Thin Films and Integrated Devices, School of Electronic Science and Engineering, University of Electronic Science and Technology of China, Chengdu 610054, China. E-mail: zqwan@uestc.edu.cn; cyjia@uestc.edu.cn*
[b]*State Key Laboratory of Applied Organic Chemistry, Lanzhou University, Lanzhou 730000, China*

† Electronic supplementary information (ESI) available: Materials, characterization method, synthetic details, DFT calculations, TGA curves, and device characterization data. See DOI: 10.1039/d1sc01416a

is also more difficult. It was also worth noting that the hole mobilities of these newly developed monospiro- and dispiro-based HTMs are also relatively low due to weak intermolecular electronic coupling caused by the molecular spatial configuration of these materials. Therefore, like Spiro-OMeTAD, these developed monospiro- and dispiro-based HTMs still require some dopants/additives (lithium bis(trifluoromethanesulfonyl)imide (Li-TFSI), *tert*-butylpyridine (*t*-BP) and cobalt complexes) to ameliorate conductivity and mobility, so that high PCEs for PSCs can finally be realized.[21] Nevertheless, it is well known that Li-TFSI is moisture-sensitive, which can directly cause perovskite film degradation, and has a negative effect on the stability of device.[22–24]

In this work, through simple and ingenious molecular structure modification, a novel dispiro-based HTM denoted as WH-1 was designed using cyclohexane to substitute the central carbon atom of Spiro-OMeTAD as shown in Fig. 1a. The spatial configuration of this HTM changes from an orthogonal conformation of the two fluorene units to a parallel arrangement (Fig. 1b). The improvement of the planarity of the two fluorene units can enhance the ordered stacking of molecules, thus enhancing the charge transfer and intrinsic hole mobility.[25] Furthermore, it is beneficial for the formation of a homogeneous and compact film coating on the perovskite film, which is of great significance for reducing the perovskite and HTM interface charge recombination, so as to improve charge collection efficiency and PSC performance.[26] WH-1 was applied as a dopant-free HTM in PSCs, and a PCE of 19.57% was obtained, which is comparable to that of Li-TFSI/*t*-BP doped Spiro-OMeTAD (20.29%). More importantly, compared to the doped Spiro-OMeTAD, PSC based on dopant-free WH-1 exhibits more excellent stability after the device was stored under dark ambient conditions with a humidity of 50–70% at room temperature for 60 days. This work is the first time, as far as we know, that the dispiro-based molecule has been applied as a dopant-free HTM in PSCs.

Results and discussion

The synthesis of the spiro core in Spiro-OMeTAD is quite challenging and requires several reaction steps including the Grignard reaction, Hartwig–Buchwald coupling reaction, and so on.[27] In contrast, owing to the simple and ingenious design of a cyclohexane linkage between the fluorene planes, the synthesis of WH-1 from commercial raw material 2,7-dibromo-9*H*-fluorene only needs a simple two-step synthesis process resulting in a total yield of more than 60%, as shown in Scheme 1. Compared with Spiro-OMeTAD, the synthetic route of WH-1 is more simple and efficient, which indicates that WH-1 has a lower synthesis expense and offers prospects for large-scale application of PSCs. In order to assess the price of the synthesized materials, we performed a cost-analysis on the lab-scale synthesis, and detailed synthetic cost evaluations are given in Table S1.† The estimated cost of WH-1 is 23.57 \$ g^{-1}, and WH-1 is considered to be a low-cost HTM in comparison with the more commonly used Spiro-OMeTAD.[28]

In order to understand the spatial configuration of WH-1, the DFT simulated molecular geometries of WH-1 and Spiro-OMeTAD are shown in Fig. 1b. The side views of the molecular geometries are exhibited in Fig. S3 in the ESI.† It can be

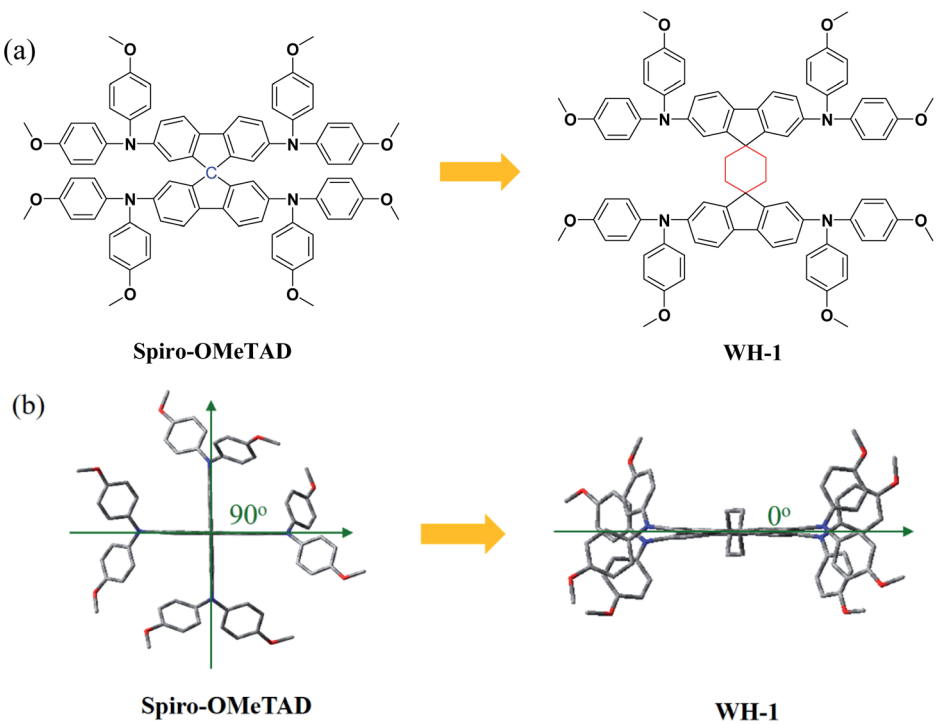

Fig. 1 (a) Molecular structures and (b) DFT simulated molecule geometries of WH-1 and Spiro-OMeTAD.

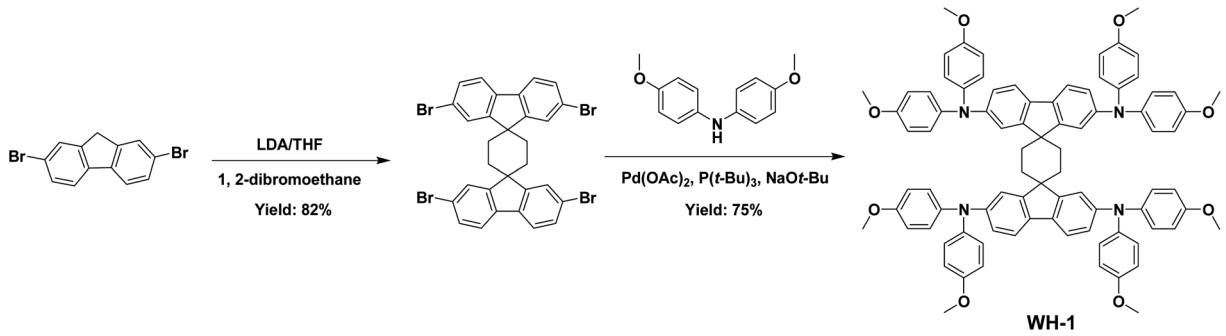

Scheme 1 The synthetic route of WH-1.

seen that the dihedral angle between the two fluorene units changed enormously from 90 degrees of Spiro-OMeTAD to zero degrees of WH-1. That is to say, the spatial configuration of two fluorene planes shifted from the perpendicular arrangement to the parallel arrangement by the introduction of cyclohexane to replace the central carbon atom of Spiro-OMeTAD. Improving the planarity of the two fluorene units is conducive to the formation of ordered stacking of WH-1 molecules, thus enhancing the charge transfer and intrinsic hole mobility.[25] Moreover, similar to Spiro-OMeTAD, the central linkage in the WH-1 structure inhibits delocalization to another fluorene unit and separates them electronically, which is validated by the electronic distribution of the highest occupied molecular orbital (HOMO) (Fig. S4†).

The normalized UV-vis absorption and photoluminescence spectra of WH-1 and Spiro-OMeTAD in CH_2Cl_2 are shown in Fig. 2a. It is found that there are strong absorption peaks at 307 and 385 nm and a shoulder peak at 369 nm in the absorption spectrum of Spiro-OMeTAD. Similarly, WH-1 exhibits two absorption peaks at 309 and 380 nm. The optical band gap (E_g) of WH-1 calculated using the crossover point of the absorption and emission spectra is 3.08 eV, which is comparable to that of Spiro-

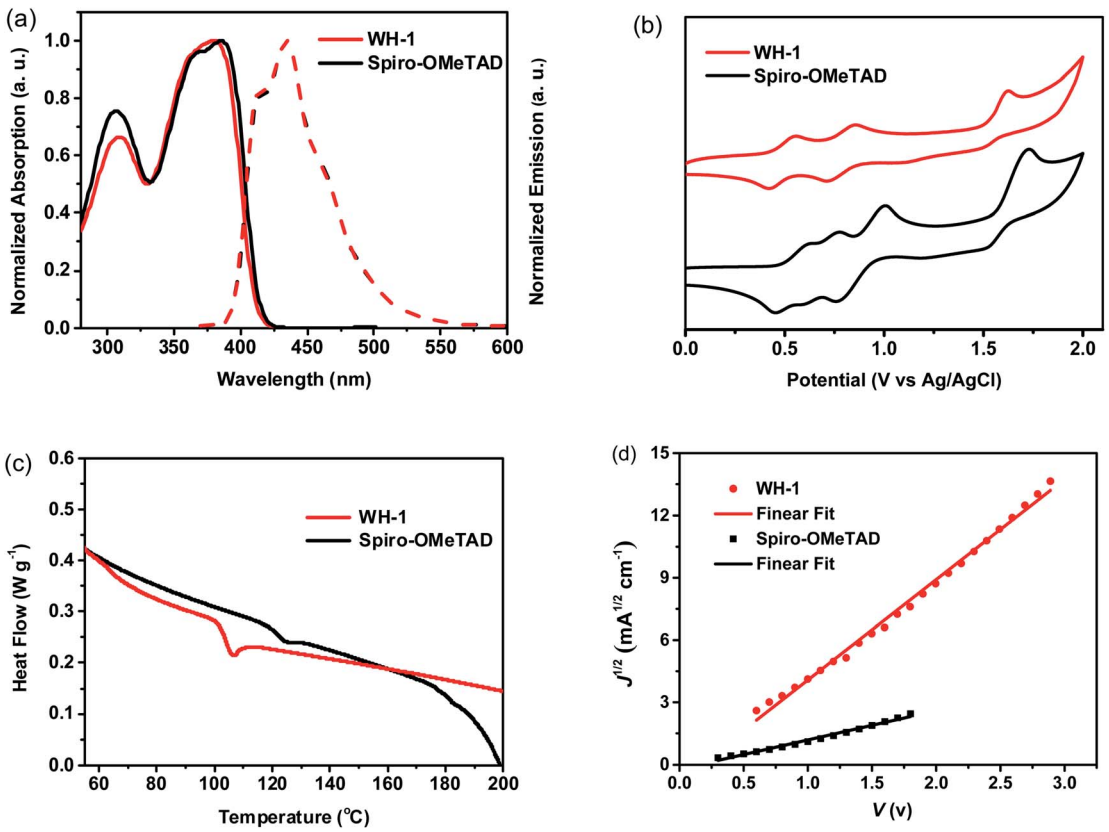

Fig. 2 (a) Normalized absorption and fluorescence spectra of WH-1 and Spiro-OMeTAD. (b) Cyclic voltammograms of WH-1 and Spiro-OMeTAD. (c) DSC curves of WH-1 and Spiro-OMeTAD at a heating rate of 10 °C min^{-1}. (d) SCLC hole-mobility curves of dopant-free WH-1 and Spiro-OMeTAD.

OMeTAD (3.07 eV). The energy levels of the HTMs were obtained from cyclic voltammetry (CV) measurements (Fig. 2b), and the relevant data are listed in Table 1. The WH-1's HOMO is calculated to be −5.14 eV, which is comparable with that of Spiro-OMeTAD (−5.19 eV). In addition, according to the HOMO and E_g, the WH-1's LUMO is −2.06 eV calculated by using the equation of $E_{LUMO} = E_{HOMO} + E_g$. These results show that the energy levels of WH-1 are matched with the perovskite, which is beneficial for the effective extraction of holes and the effective blocking of

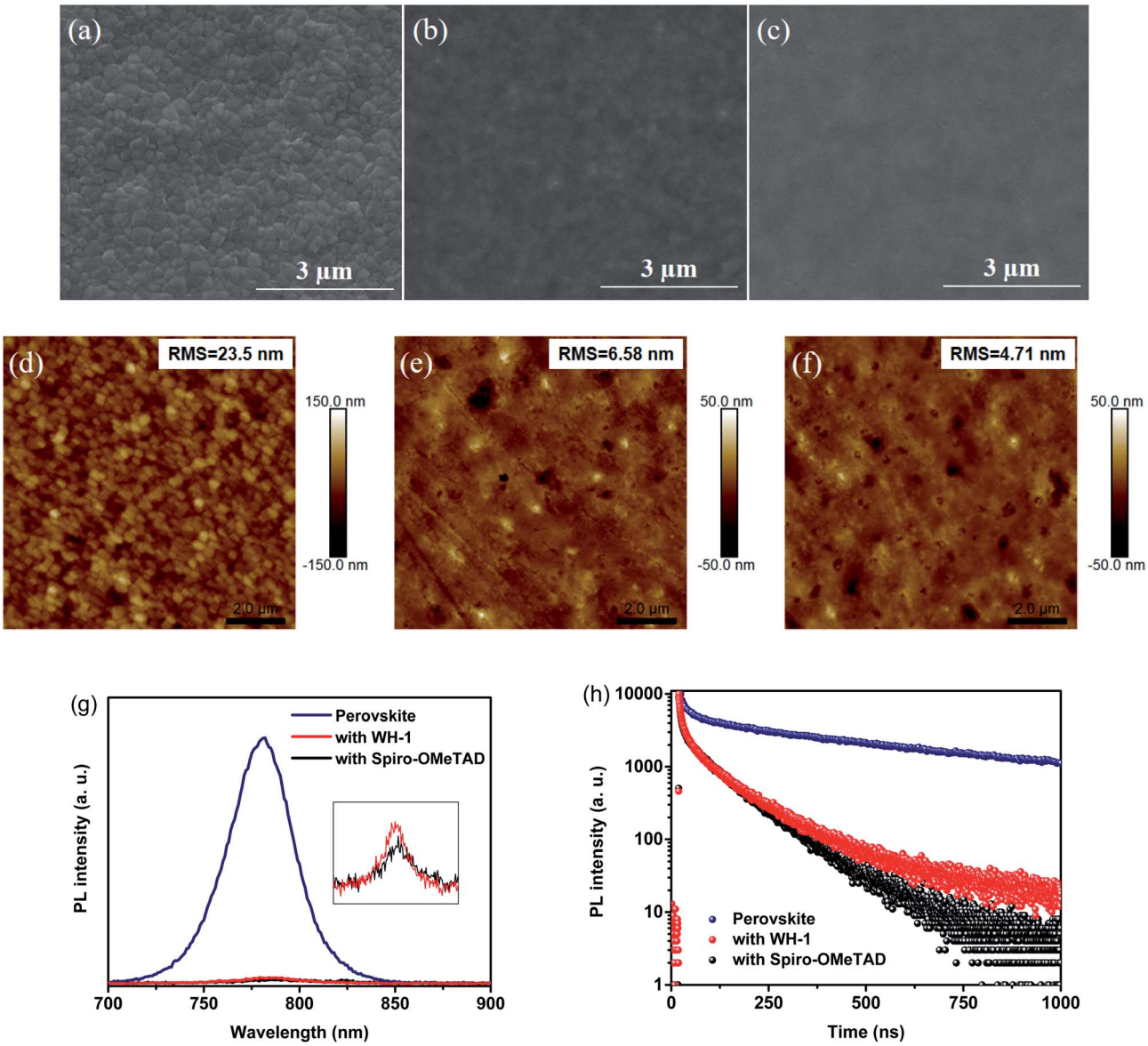

Fig. 3 SEM and AFM images of the bare perovskite (a and d), perovskite/doped Spiro-OMeTAD (b and e), perovskite/WH-1 (c and f), respectively. (g) Steady-state PL spectra of the perovskite films with and without HTMs. (h) TRPL decay of the perovskite films with and without HTMs.

Table 1 The energy level, and thermal and hole mobility data of the HTMs

HTMs	E_g[a] [eV]	E_{HOMO}[b] [eV]	E_{LUMO}[c] [eV]	T_g[d] [°C]	μ_h[e] [$cm^2\ V^{-1}\ s^{-1}$]
WH-1	3.08	−5.14	−2.06	107	3.50×10^{-5}
Spiro-OMeTAD	3.07	−5.19	−2.12	124	1.46×10^{-6}

[a] E_g calculated according to the intersection of the normalized absorption and fluorescence spectra in CH_2Cl_2. [b] Calculated from the onset oxidation potentials obtained from the CV curves. [c] Calculated by using the equation of $E_{LUMO} = E_{HOMO} + E_g$. [d] Glass transition temperature determined by DSC experiments performed at a scan rate of 10 °C min^{-1}. [e] Measured by the device structure of ITO/PEDOT:PSS/HTL/MoO_3/Al.

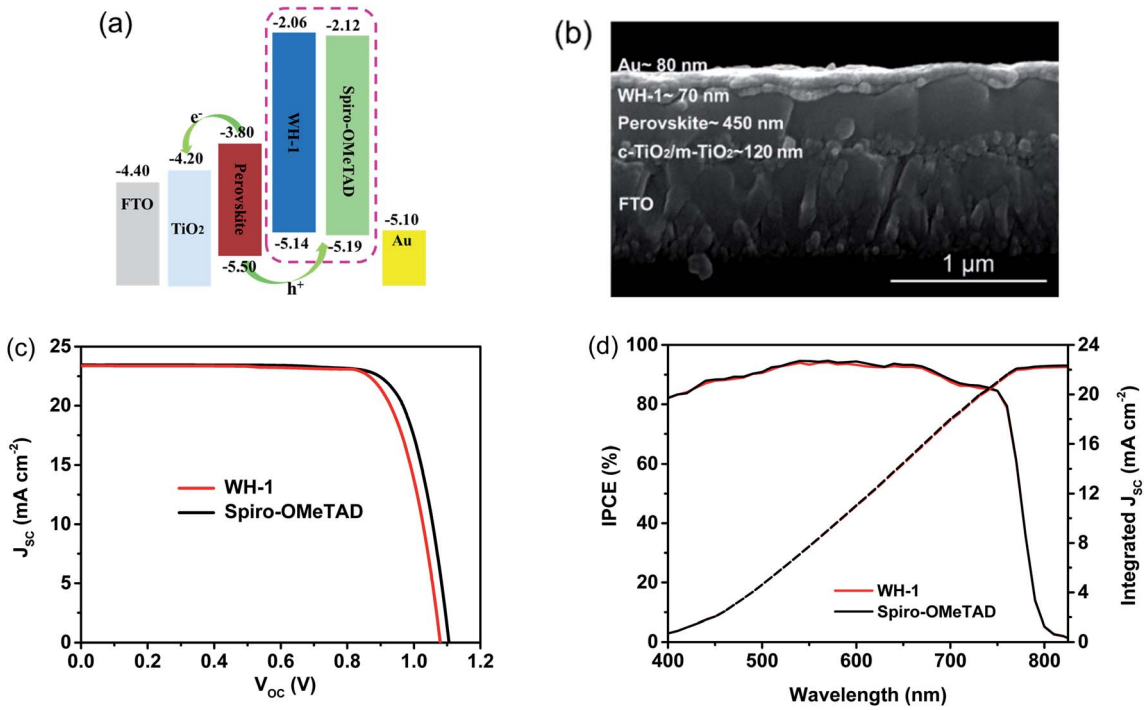

Fig. 4 (a) Schematic diagram of the energy levels of each part in the PSCs. (b) SEM image of the cross section of the whole device. (c) The *J*–*V* curves with reverse scanning for the champion PSCs based on WH-1 and Spiro-OMeTAD. (d) IPCE spectra of the PSCs based on WH-1 and Spiro-OMeTAD.

electrons. The energy-level diagram based on the above data is displayed in Fig. 4a.

Thermogravimetric analysis (TGA) and differential scanning calorimetry (DSC) are used to study the thermal properties of WH-1. Based on the TGA curves (Fig. S5†), we know that WH-1 has a high decomposition temperature (T_{dec}) of 416 °C with 5% weight loss, demonstrating that the thermal stability of WH-1 meets the needs of photovoltaic devices. Moreover, the glass transition temperature (T_g) of WH-1 is 107 °C from the second heating scan (Fig. 2c), indicating that the HTM is completely amorphous and is expected to form a uniform film in PSC devices.

The hole transporting ability of a HTM is a significant index for evaluating its application prospects in PSCs. The hole mobility of WH-1 was measured using the space charge limited current (SCLC) method with a device structure of ITO/PEDOT:PSS/HTM/MoO_3/Al. The hole mobility of 3.50×10^{-5} $cm^2\ V^{-1}\ s^{-1}$ for WH-1 was obtained as displayed in Fig. 2d, which is better than that of dopant-free Spiro-OMeTAD (1.46×10^{-6} $cm^2\ V^{-1}\ s^{-1}$). One thing to note is that an HTM layer of only a few nanometers to tens of nanometers in thickness is needed for dopant-free PSCs, and a mobility greater than 1.0×10^{-5} $cm^2\ V^{-1}\ s^{-1}$ is enough to transmit charge carriers vertically to the anode without loss of resistance.[29]

From the scanning electron microscopy (SEM) results of the perovskite film (Fig. 3a), we know that the crystal size ranges from 200 to 300 nm. The HTMs were then spun onto the perovskite film and the surface morphologies of hole transport layers were studied. The uniformity of the doped Spiro-OMeTAD film is slightly poorer (Fig. 3b) as reported in the literature[26] while the dopant-free WH-1 film coated on a perovskite layer is highly homogeneous (Fig. 3c). It is clear that the more homogeneous surface of the WH-1 film is due to the parallel arrangement of two fluorene units in the molecular structure. The atomic force microscopy (AFM) results (Fig. 3d–f) show the same trend as that observed in SEM (Fig. 3a–c). The surface roughness (RMS) of the perovskite layer was 23.5 nm. After spin coating the HTMs on top of the perovskite layer, the RMS values of the HTM-coated films were significantly decreased with the order of doped Spiro-OMeTAD (6.58 nm) > WH-1 (4.71 nm). Compared with the Spiro-OMeTAD film, the coverage of the WH-1 film on the perovskite surface is more uniform, which is of great significance for reducing the charge recombination loss of the perovskite and HTM interface in PSCs, improving charge collection efficiency and photovoltaic performance.[26] Although the hole mobility was moderate, the WH-1 film without any dopants can ensure effective holes transport benefitting from its excellent film quality.

The hole-extraction capability of WH-1 was studied by means of steady-state photoluminescence (PL) and time-resolved photoluminescence (TRPL). Fig. 3g displays the PL spectra of perovskite films, without or with a HTM layer. A broad PL band centered at 780 nm was observed under 460 nm excitation for the pristine perovskite film. Compared with the bare perovskite film, the emission intensities of each HTM coating decreased significantly. About 96.61% of the emission is quenched on the dopant-free WH-1-coated perovskite film, which is comparable to that of doped Spiro-OMeTAD (97.33%). This quenching

indicates that dopant-free WH-1 can effectively extract the holes produced in the perovskite layer,[27] and the hole extraction ability of dopant-free WH-1 is almost the same as that of doped Spiro-OMeTAD, which is further supported by TRPL measurements. The TRPL results show that the average decay time (τ_{avg}) of the pristine perovskite film is 474 ns (Fig. 3h). The τ_{avg} values of doped Spiro-OMeTAD and dopant-free WH-1 decreased significantly to 34.1 ns and 37.9 ns, respectively. The relatively short lifetime is clearly observed for the perovskite film covered with WH-1, which is equivalent to that of Spiro-OMeTAD. It means that WH-1 can effectively extract holes and retard trap induced nonradiative carrier recombination.[30] The parallel arrangement structure of two fluorene planes in WH-1 leads to better electronic contact between the perovskite and WH-1, which promotes effective hole transfer and extraction.[26] Based on the above discussion, WH-1 as a dopant-free HTM has great application potential in PSCs.

Furthermore, to investigate the actual performance of WH-1 as a dopant-free HTM, a PSC device was fabricated with a structure of glass/FTO/c-TiO_2 (~20 nm)/m-TiO_2 (~100 nm)/perovskite (~450 nm)/WH-1 (~70 nm)/Au (~80 nm). The cross sectional SEM image of the whole device is shown in Fig. 4b. Since the concentrations of the HTM are critically important in determining the photovoltaic performances, we first tried to find the best concentration of WH-1 in the PSCs. The concentration was optimized using current density–voltage (*J–V*) curves, as demonstrated in Fig. S6,† and the related parameters are summarized in Table S2.† Among them, the PSC with WH-1 exhibited the best performance when spin-coated with a concentration of 20 mg mL^{-1} in chlorobenzene.

Fig. 4c shows the *J–V* curves of champion PSCs containing Spiro-OMeTAD and WH-1, and the summarized PSC parameters are listed in Table 2. As a standard, the PSC with doped Spiro-OMeTAD exhibits a PCE of 20.29%, with a short-circuit density (J_{sc}) of 23.46 mA cm^{-2}, an open circuit voltage (V_{oc}) of 1.11 V, and a fill factor (FF) of 77.94%. Under the same circumstances, the dopant-free WH-1-based PSC reaches a PCE of 19.57%, with J_{sc} = 23.37 mA cm^{-2}, V_{oc} = 1.08 V, and FF = 77.54%, which are comparable with the parameters of the doped Spiro-OMeTAD based device. Compared with the PSC based on doped Spiro-OMeTAD, the V_{oc} of the PCS based on dopant-free WH-1 is lower because of its upshifted HOMO level.[31] Additionally, compared with the PSC based on doped Spiro-OMeTAD, the *J–V* curves of the PSC with dopant-free WH-1 at forward and reverse scanning show smaller hysteresis (Fig. S7, S8 and Table S3†). The PCEs of PSCs based on dopant-free WH-1 and doped Spiro-OMeTAD were tested using 30 devices for each HTM. The statistical data are shown in the ESI (Fig. S9†). It is clear that the devices show good reproducibility and the average PCE of the devices with dopant-free WH-1 is 19.17 ± 0.39%, which is comparable to that of devices with doped Spiro-OMeTAD (19.80 ± 0.48%).

The integrated current densities calculated according to the incident photon-to-current conversion efficiency (IPCE) spectra (Fig. 4d) of the dopant-free WH-1 and doped Spiro-OMeTAD based PSCs are 22.31 and 22.43 mA cm^{-2}, respectively, which are in good agreement with J_{SC} values from the *J–V* curves. The photovoltaic results directly confirm the feasibility of WH-1 as a dopant-free HTM for efficient PSCs. Importantly, the optimal concentration of WH-1 solution for the hole-transporting layer preparation is only 20 mg mL^{-1}, much lower than that of Spiro-OMeTAD (72.3 mg mL^{-1}), which not only reduces the consumption and cost, but also shortens the transmission distance of holes from the perovskite to the anode.[29] In short, a thinner hole-transporting layer with effective extraction of holes and good surface coverage ensures the high PCE of a PSC based on dopant-free WH-1, although it has only a moderate hole mobility.

Fig. 5a shows the stabilized photocurrent and PCE of the PSC based on dopant-free WH-1 at the maximum power point within 200 s. The stable PCE output of the PSC based on dopant-free WH-1 is 19.52%, and the photocurrent is 22.43 mA cm^{-2}, respectively. The results show that the *J–V* curve of the PSC is reliable. Furthermore, we tested the stability of unpackaged PSCs with dopant-free WH-1 and doped Spiro-OMeTAD stored under dark ambient conditions with a humidity of 50–70% at room temperature depending on the *J–V* curves (Fig. 5b). The dopant-free WH-1 based PSC exhibits much better stability than the device based on doped Spiro-OMeTAD. After 60 days, the doped Spiro-OMeTAD based PSC retained only 37% of initial PCE. However, dopant-free WH-1 based PSCs still retained 87% of the original PCE under the same conditions. The hydrophilic property of the HTM film was tested to discuss its effect on device stability. The water contact angles of the films with dopant-free WH-1 and doped Spiro-OMeTAD were 88.4° and 66.2° (Fig. 5b), respectively. Dopant-free WH-1 has better hydrophobicity, and can offer a more effective moisture-proof layer than doped Spiro-OMeTAD, so that PSCs based on dopant-free WH-1 have better long-term stability. But beyond that, the relatively stable performance of a WH-1-based device is also attributed to the formation of a uniform and smooth WH-1 coating layer on the

Table 2 Summary parameters of champion PSCs with dopant-free WH-1 and doped Spiro-OMeTAD[a]

HTMs	J_{sc} [mA cm^{-2}]	V_{oc} [V]	FF [%]	Best PCE [%]	Average PCE[c] [%]
WH-1	23.37 (22.31)	1.08	77.54	19.57	19.17 ± 0.39
Spiro-OMeTAD[b]	23.46 (22.43)	1.11	77.94	20.29	19.80 ± 0.48

[a] Measured under AM 1.5G (100 mW cm^{-2}). [b] Doped by Li-TFSI/*t*-BP. [c] The average PCE values of 30 PSC devices. Note: the J_{sc} values in the parentheses are the integrated values based on IPCE measurements.

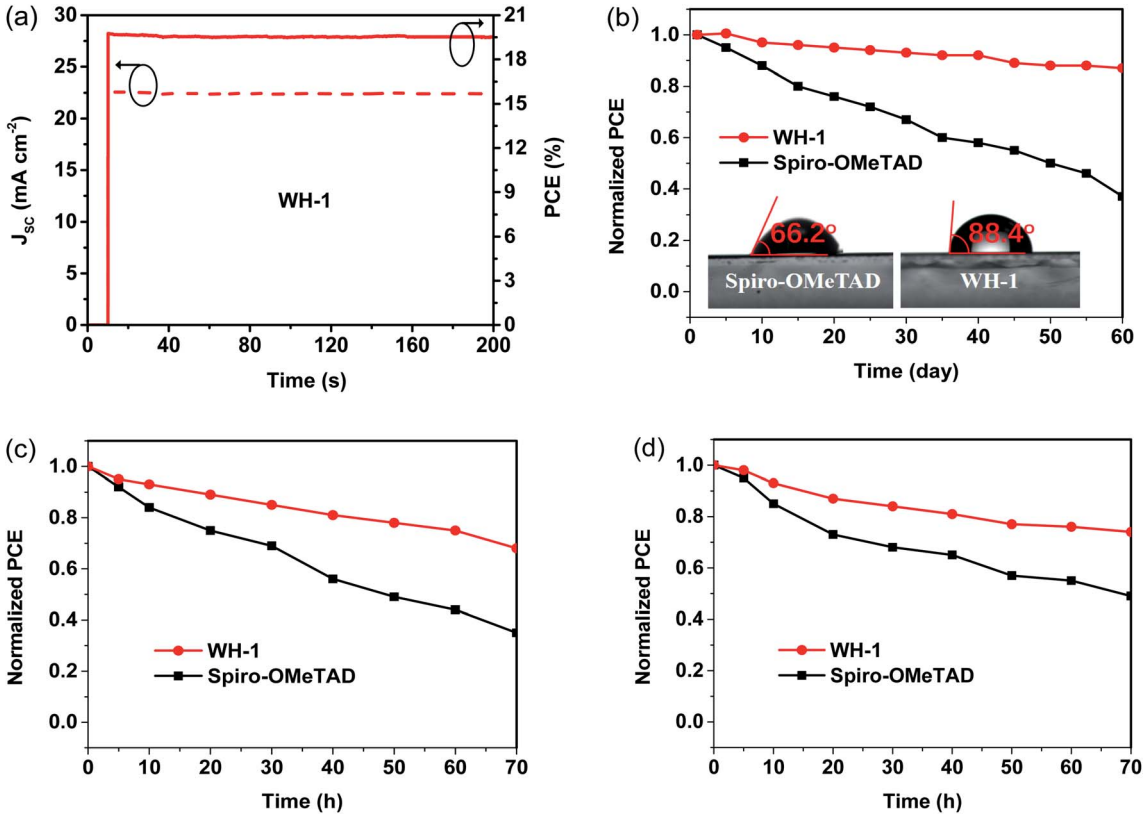

Fig. 5 (a) The steady-state photocurrent and PCE of a PSC with dopant-free WH-1 at the maximum power output of 0.87 V. (b) Stability tests of PSCs with dopant-free WH-1 and doped Spiro-OMeTAD under dark ambient conditions with a humidity of 50–70% at room temperature. Inset: water contact-angle tests of perovskite/Li-TFSI/*t*-BP doped Spiro-OMeTAD and perovskite/dopant-free WH-1 films. (c) Thermal stability of PSCs with dopant-free WH-1 and doped Spiro-OMeTAD at a constant 85 °C in an ambient environment. (d) Light stability of PSCs with dopant-free WH-1 and doped Spiro-OMeTAD under continuous 1 sun equivalent illumination in an ambient environment.

perovskite film, which prevents moisture from entering the perovskite layer (Fig. 3c and f).

Additionally, we also monitored the thermal stability of unpackaged PSCs with dopant-free WH-1 and doped Spiro-OMeTAD at a constant 85 °C in an ambient environment. As shown in Fig. 5c, approximately 68% of the initial PCE is retained for the PSC based on dopant-free WH-1 after 70 h, whereas the PCE of the doped Spiro-OMeTAD-based PSC drops to 35%. Lastly, the light stability of PSCs with dopant-free WH-1 and doped Spiro-OMeTAD under continuous 1 sun equivalent illumination in an ambient environment was studied as shown in Fig. 5d. The retained PCE of 74% for the dopant-free WH-1-based PSC was much higher than that (49%) of the doped Spiro-OMeTAD-based PSC. Thus, the dopant-free WH-1 based PSC not only has a PCE as high as that of the doped Spiro-OMeTAD based PSC, but also has good device stability.

Conclusions

In summary, a novel dispiro-based molecule WH-1 was designed and synthesized, which has a parallel arrangement structure of two fluorene units. This feature is beneficial for the formation of a homogeneous and compact HTM film, improvement of intermolecular electronic coupling and intrinsic hole mobility. Compared to doped Spiro-OMeTAD, the PSC based on WH-1 as the dopant-free HTM exhibits comparable efficiency, and also enhances device stability. Moreover, WH-1 has a lower synthesis cost and less consumption, thus reducing the total cost per unit area of the PSC device. Therefore, the advantages of WH-1 in terms of cost, efficiency and stability make it a potential HTM for further development of PSCs. This work is the first time as far as we know that the dispiro-based molecule has been used as a dopant-free HTM in PSCs and provides a design idea for the development of novel spiro-based HTMs.

Author contributions

Z. Wan conceived the idea of the article. Z. Wan synthesized the relevant materials. Z. Wan, J. Yang, H. Shu and J. Luo fabricated and characterized the devices. J. Xia and X. Yao performed DFT calculation. Z. Wan wrote and revised the manuscript. C. Jia supervised the project.

Conflicts of interest

There are no conflicts to declare.

Acknowledgements

The authors are grateful to the Sichuan Science and Technology Program (Grant nos. 2019YJ0162 and 2020YJ0029), National Natural Science Foundation of China (Grant nos. 21572030 and 51773027) and National Key R@D Program of China (Grant no. 2017YFB0702802) for financial support.

References

1 A. Kojima, K. Teshima, Y. Shirai and T. Miyasaka, *J. Am. Chem. Soc.*, 2009, **131**, 6050–6051.
2 J. Burschka, N. Pellet, S.-J. Moon, R. Humphry-Baker, P. Gao, M. K. Nazeeruddin and M. Grätzel, *Nature*, 2013, **499**, 316–319.
3 Q. Jiang, Y. Zhao, X. Zhang, X. Yang, Y. Chen, Z. Chu, Q. Ye, X. Li, Z. Yin and J. You, *Nat. Photonics*, 2019, **13**, 460–466.
4 National Renewable Energy Laboratory, *Best research-cell efficiencies chart*, 2020, www.nrel.gov/pv/assets/pdfs/best-research-cell-efficiencies.20200218.pdf.
5 G.-W. Kim, H. Choi, M. J. Kim, J. W. Lee, S. Y. Son and T. Park, *Adv. Energy Mater.*, 2020, **10**, 1903403.
6 H. Zhang, Y. Wu, W. Zhang, E. Li, C. Shen, H. Jiang, H. Tian and W. Zhu, *Chem. Sci.*, 2018, **9**, 5919–5928.
7 B. Pashaei, S. Bellani, H. Shahroosvand and F. Bonaccorso, *Chem. Sci.*, 2020, **11**, 2429–2439.
8 N. J. Jeon, H. Na, E. H. Jung, T.-Y. Yang, Y. G. Lee, G. Kim, H.-W. Shin, S. I. Seok, J. Lee and J. Seo, *Nat. Energy*, 2018, **3**, 682–689.
9 D. P. Tabor, V. A. Chiykowski, P. Friederich, Y. Cao, D. J. Dvorak, C. P. Berlinguette and A. Aspuru-Guzik, *Chem. Sci.*, 2019, **10**, 8360–8366.
10 N. Xu, A. Zheng, Y. Wei, Y. Yuan, J. Zhang, M. Lei and P. Wang, *Chem. Sci.*, 2020, **11**, 3418–3426.
11 P. Ganesan, K. Fu, P. Gao, I. Raabe, K. Schenk, R. Scopelliti, J. Luo, L. H. Wong, M. Grätzel and M. K. Nazeeruddin, *Energy Environ. Sci.*, 2015, **8**, 1986–1991.
12 Z. Hu, W. Fu, L. Yan, J. Miao, H. Yu, Y. He, O. Goto, H. Meng, H. Chen and W. Huang, *Chem. Sci.*, 2016, **7**, 5007–5012.
13 D. Bi, B. Xu, P. Gao, L. Sun, M. Grätzel and A. Hagfeldt, *Nano Energy*, 2016, **23**, 138–144.
14 B. Xu, D. Bi, Y. Hua, P. Liu, M. Cheng, M. Grätzel, L. Kloo, A. Hagfeldt and L. Sun, *Energy Environ. Sci.*, 2016, **9**, 873–877.
15 M. Saliba, S. Orlandi, T. Matsui, S. Aghazada, M. Cavazzini, J.-P. Correa-Baena, P. Gao, R. Scopelliti, E. Mosconi, K.-H. Dahmen, F. De Angelis, A. Abate, A. Hagfeldt, G. Pozzi, M. Grätzel and M. K. Nazeeruddin, *Nat. Energy*, 2016, **1**, 15017.
16 J. Zhang, B. Xu, L. Yang, C. Ruan, L. Wang, P. Liu, W. Zhang, N. Vlachopoulos, L. Kloo, G. Boschloo, L. Sun, A. Hagfeldt and E. M. J. Johansson, *Adv. Energy Mater.*, 2018, **8**, 1701209.
17 K. Gao, B. Xu, C. Hong, X. Shi, H. Liu, X. Li, L. Xie and A. K. Y. Jen, *Adv. Energy Mater.*, 2018, **8**, 1800809.
18 D. Y. Lee, G. Sivakumar, Manju, R. Misra and S. I. Seok, *ACS Appl. Mater. Interfaces*, 2020, **12**, 28246–28252.
19 N. Drigo, C. Roldan-Carmona, M. Franckevičius, K. Lin, R. Gegevičius, H. Kim, P. A. Schouwink, A. A. Sutanto, S. Olthof, M. Sohail, K. Meerholz, V. Gulbinas, C. Corminboeuf, S. Paek and M. K. Nazeeruddin, *J. Am. Chem. Soc.*, 2020, **142**, 1792–1800.
20 X. Sallenave, M. Shasti, E. H. Anaraki, D. Volyniuk, J. V. Grazulevicius, S. M. Zakeeruddin, A. Mortezaali, M. Grätzel, A. Hagfeldt and G. Sini, *J. Mater. Chem. A*, 2020, **8**, 8527–8539.
21 N. D. Pham, J. Shang, Y. Yang, M. T. Hoang, V. T. Tiong, X. Wang, L. Fan, P. Chen, L. Kou, L. Wang and H. Wang, *Nano Energy*, 2020, **69**, 104412.
22 Y. Dong, J. Zhang, Y. Yang, L. Qiu, D. Xia, K. Lin, J. Wang, X. Fan and R. Fan, *Angew. Chem., Int. Ed.*, 2019, **58**, 17610–17615.
23 J. Luo, F. Lin, J. Xia, H. Yang, R. Zhang, H. Malik, H. Shu, Z. Wan, K. Han, R. Wang, X. Yao and C. Jia, *Nano Energy*, 2021, **82**, 105751.
24 X. Sun, F. Wu, C. Zhong, L. Zhu and Z. Li, *Chem. Sci.*, 2019, **10**, 6899–6907.
25 C. Shen, Y. Wu, H. Zhang, E. Li, W. Zhang, X. Xu, W. Wu, H. Tian and W. Zhu, *Angew. Chem., Int. Ed.*, 2019, **58**, 3784–3789.
26 J. Zhang, Y. Hua, B. Xu, L. Yang, P. Liu, M. B. Johansson, N. Vlachopoulos, L. Kloo, G. Boschloo, E. M. J. Johansson, L. Sun and A. Hagfeldt, *Adv. Energy Mater.*, 2016, **6**, 1601062.
27 T. P. I. Saragi, T. Spehr, A. Siebert, T. Fuhrmann-Lieker and J. Salbeck, *Chem. Rev.*, 2007, **107**, 1011–1065.
28 J&K Scientific, https://www.jk-scientific.com.
29 X. Wang, J. Zhang, S. Yu, W. Yu, P. Fu, X. Liu, D. Tu, X. Guo and C. Li, *Angew. Chem., Int. Ed.*, 2018, **57**, 12529–12533.
30 J. Wang, H. Zhang, B. Wu, Z. Wang, Z. Sun, S. Xue, Y. Wu, A. Hagfeldt and M. Liang, *Angew. Chem., Int. Ed.*, 2019, **58**, 15721–15725.
31 K. Jiang, J. Wang, F. Wu, Q. Xue, Q. Yao, J. Zhang, Y. Chen, G. Zhang, Z. Zhu, H. Yan, L. Zhu and H. Yip, *Adv. Mater.*, 2020, **32**, 1908011.